理學碩士 學位 論文

Pd-Pt Ultrathin Assembled Hierarchical Flower for Enhanced Ethanol Oxidation Reaction

(에탄올 산화 반응의 활성을 높이기 위한

팔라듐-백금 얇은 집합 계층적 꽃송이 촉매)

蔚 山 大 學 校 大 學 院

化 學 科

韓 藝 智

Pd-Pt Ultrathin Assembled Hierarchical Flower for Enhanced Ethanol Oxidation Reaction

指 導 敎 授 홍 종 욱

이 論文을 理學碩士 學位 論文으로 제출함

2020年 02月

蔚 山 大 學 校 大 學 院

化 學 科

韓 藝 智

韓 藝 智의 理學碩士 學位 論文을 認准함

審査委員 이 민 형 印

審査委員 홍 종 욱 印

審査委員 하 지 원 印

蔚 山 大 學 校 大 學 院

2020年 02月

국문요약

화석연료는 현재까지도 사용되는 주요 에너지원으로 40-100년 안에 화석연료가 고갈될 것으로 예상된다. 따라서 화석연료를 대체할 에너지원이 필요하며, 높은 에너지를 내면서 친환경적이고 재생가능한 에너지원이 연구되고 있다. 대체 에너지원으로 전기, 수소, 물 등이 있으며, 이들을 생산하는 반응으로 연료 산화 반응, 수소 생성 반응, 이산화탄소 환원 반응 등이 있다. 이 중 전기에너지를 생산하는 에탄올 산화 반응은 촉매가 필수적이며, 백금이 대표적이다. 하지만 백금의 높은 시장가격과 낮은 매장량으로 백금과 비슷한 성질을 가진 팔라듐이 대체되고 있다.

금속 촉매의 활성을 높이기 위한 방법에는 모양 조절, 조성 조절, 크기조절 등이 있다. 이 연구의 목적은 모양과 조성을 조절하여 알칼리성 용매 중 에탄올 산화반응에서 촉매의 활성을 높이는 것이다. 이 연구는 입자를 중심으로 시트가 자라난 계층적 꽃송이 모양의 팔라듐-백금 합금을 제시하여 활성을 높였다.

주사 전자 현미경과 투과 전자 현미경을 통해 Pd-Pt 집합 나노시트의 계층적 꽃송이 모양을 확인하였다. 또한 HAADF-STEM-EDS을 통해 팔라듐과 백금의 균일성을 확인하였으며, 유도결합 플라즈마-광학적 발광 광도계를 통하여 이들의 조성 (Pd:Pt, 10:1)을 확인하였다. 그리고 X-ray 회절 분석법을 통하여 촉매의 fcc 구조를 확인하였다.

KI, CTAC 그리고 AA는 계층적 꽃송이 모양을 형성하는 중요한 요소이다. KI는 [111]방향에서의 팔라듐과 백금의 성장을 억제하여 2차원적인 구조를 형성한다. CTAC는 계면활성제이다. AA는 환원제로 금속 이온의 환원 속도를 조절한다. CTAC와 AA는 과량이 들어갈 경우 아이오다이드 (I^-) 이온의 흡착을 방해하여 불규칙한 모양의 3차원적 나노 입자를 형성한다.

시약의 특성을 이용하여 모양에 대한 대조군으로 동일한 조성을 가진 Pd-Pt 나노 크리스탈 (NCs)을 합성하였다. 그리고 조성에 대한 대조군으로 상업적으

로 판매하는 Pd/C와 Pt/C를 선택하였다. 총 4가지 촉매의 알칼리성 용액 중 에탄올 산화 반응에 대한 전기화학적 특성을 확인한 결과, Pd-Pt 얇은 집합 나노시트는 0.5 KOH + 1.0 M 에탄올 조건에서 3369 mA mg^{-1}의 높은 질량 활성(Pd-Pt 나노 크리스탈보다 1.91배, Pd/C보다 2.36배 그리고 Pt/C보다 2.71배)을 나타냈다. 그리고 Pd-Pt 얇은 집합 나노시트는 0.5 KOH + 1.0 M 에탄올 조건에서 순환 전류법 300 바퀴 후에 70% 이상의 활성을 유지하였고, 좋은 안정성을 보여주었다. 이 실험을 통해 촉매의 모양과 조성이 전기화학적 특성에 영향을 주는 큰 요인임을 확인할 수 있었다.

Abstract

In the past decade, fossil fuels are the main energy source. They are expected to be depleted in 40-100 years. Therefore, energy sources to replace fossil fuels are needed. Recently, eco-friendly and renewable energy sources with high energy are being researched. To produce alternative energies, fuel oxidation, hydrogen evolution and carbon dioxide reduction reaction systems are used. Among the fuel oxidation systems, ethanol oxidation reaction could produce electrochemical energy. To increase the effectivity of EOR, it needs catalyst. Platinum is representative for using as catalyst. However, platinum has been replaced by palladium because of the high market price and scarce of sources.

There are various ways to increase the activity of metal catalysts such as shape, size and controlled compositional structure. The purpose of this study is to improve the activity of catalysts in ethanol oxidation reaction in alkaline media by modified their morphology and composition. This study designed the alloy nanocrystal with hierarchical flower shape with the sheet growing around the particles to enhance the activity of catalyst.

Their hierarchical shape of Pd-Pt nanocrystal was confirmed by scanning electron microscopy (SEM) and transmission electron microscopy (TEM). In addition, the uniform distribution of palladium and platinum and composition (Pd:Pt, 10:1) were identified through HAADF-STEM-EDS and ICP-OES, respectively. Their face-centered cubic (fcc) structure was identified by X-ray diffraction spectroscopy (XRD).

KI, CTAC and AA are critical factors in forming hierarchical flower shape. KI inhibits the growth of palladium and platinum in the [111] orientation, forming a two-dimensional structure. CTAC is a surfactant. AA is a reducing agent that controls the rate of reduction of metal ions. When using excess CTAC and AA, they interfere the adsorption of iodide (I^-), forming irregularly shaped three-dimensional nanoparticles.

Ethanol oxidation reaction in alkaline solution were conducted for 4 kinds of catalyst (Pd-Pt ultrathin assembled nanosheet, Pd-Pt irregular shaped nanocrystals, commercial Pd/C and Pt/C). Pd-Pt irregular shaped nanocrystals (IS NCs) was a control group for the morphology. Commercial Pd/C and Pt/C catalysts were used for comparing the catalysts activity for composition. In EOR activity, Pd-Pt ultrathin assembled nanosheets (UANs) showed the

highest mass activity of 3369 mA mg^{-1} (1.91 times higher than Pd-Pt IS NCs, 2.36 times higher than Pd/C and 2.71 times higher than Pt/C). In addition, after 300 cycles of CVs under the same conditions, the mass activity of Pd-Pt ultrathin assembled nanosheets maintained more than 70%. This study confirmed that the morphology and composition of the catalyst is a significant factor affecting the electrochemical properties.

Index

I. Introduction

Until now, fossil fuels are using as the main energy source in the world. One paper suggests that the fossil fuel time depletion is calculated to be around 35, 107 and 37 years for oil, coal and gas, respectively, which will increase the price of fuel due to limited reserves.[1] It indicates the importance of developing the sustainable energy sources instead of fossil fuels.[2] Recently, many researchers are investigating alternative energy sources that are environment, low-toxic, renewable with high power density.[2-3] For alternative energy source, there are many things such as electricity, hydrogen and water. For producing them, fuel oxidation reaction, hydrogen evolution reaction, carbon dioxide reduction and water splitting reaction and so on are used. Among them, the ethanol oxidation reaction (EOR) is the way to produce energy from ethanol using a polymer electrolyte membrane fuel cell (PEMFC) over an anodic electrocatalyst.[2] PEMFC uses polymer membrane with hydrogen ion exchange ability as electrolyte, so that there is no loss of electrolyte and it is possible to apply the existing reforming technology such as methanol reforming. Also, it has many advantages: low activating temperature, high efficiency, high current density, high power density and fast responsibility.[4-5] In EOR, platinum (Pt) which is suitable for the oxidation of hydrogen and the reduction of oxygen is mainly used as the catalyst.[6] However, platinum is too expensive than other catalyst and the reserve is low. Recently, because of the high price and scarce of platinum source, palladium has a promising alternative metal to reduce price and consume of platinum.[7-10] Also, palladium is using as catalyst rather than platinum due to electrochemical properties. It has been revealed that palladium nanoparticles (NPs) show better performance in formic acid oxidation at the anode of polymer electrolyte membrane fuel cells (PEMFCs) than platinum catalysts owing to their greater resistance to carbon monoxide (CO) poisoning.[11-13] Palladium has also been reported to have a higher electrocatalytic activity than platinum toward ethanol oxidation in alkaline media because it has a slightly better ability to break the C-C bond of ethanol in high pH media compared to platinum-based catalysts.[14-18] Additionally, there are universal ways to increase the activity of palladium catalyst. By adjusting the morphology and composition of Pd catalyst, the activity can be increased.[19-26]

Herein, we report the appropriate synthesis method for the formation of Pd-Pt ultrathin assembled nanosheets (UANs) with low-coordinated and Pd-Pt alloy surfaces. The bimetallic

composition and wide active surface areas will increase the activity of catalyst in ethanol oxidation reaction (EOR) in alkaline solution. This study demonstrates that the morphology and composition effect on the electrocatalytic properties of catalyst toward EOR.

II. Experimental

Chemicals and materials. Potassium tetrachloropalladate (ll) (K_2PdCl_4, 98%), potassium tetrachloroplatinate (ll) (K_2PtCl_4, 98%), potassium iodide (KI, ≥99.0%), cetyltrimethylammonium chloride (CTAC, 25 wt% in H_2O) and nafion ® perfluorinated resin solution (5 wt%) were obtained from Sigma-Aldrich, Palladium on activated carbon (Pd/C, 20 wt%) and platinum on carbon black (Pt/C, 20 wt%) were obtained from Alfa aesar. Potassium hydroxide (KOH, 95.0%) was obtained from Samchun. L-ascorbic acid (AA, 99.5%) was obtained from Daejung. Other chemicals were reagent grade, and deionized water with a resistivity of greater than 18.3 MΩ·cm was used in the preparation of reaction solutions.

Synthesis of Pd-Pt ultrathin assembled nanosheets. In a typical synthesis of assembled Pd-Pt ultrathin assembled nanosheets, aqueous solutions of KI (0.8 mL, 50 mM), K_2PdCl_4 (0.2 mL, 7.66 mM), K_2PtCl_4 (0.02 mL, 7.66 mM), and AA (0.2 mL, 50 mM) were sequentially injected into an aqueous solution of CTAC (1 mL, 5 mM). Then, the reaction solution was heated at 100 °C oven for 5 h. The product was washed twice with deionized water and ethanol mixture by centrifugation at 6,000 rpm for 5 min.

Characterization. TEM and SEM images of the prepared catalysts were obtained by using a JEOL JEM-2100F and a JEOL JEM-7210F, respectively. TEM measurements were conducted after placing a drop of the hydrosol on a carbon-coated Cu grid (300 mesh). The compositions of nanostructures were determined by inductively coupled plasma-optical emission spectrometry (ICP-OES, Spectroblue-ICP-OES (Ametek)). X-ray diffraction (XRD) measurement were conducted on a Rigaku D/MAX2500V/PC using Cu K_α(0.1542 nm) radiation.

Electrochemical measurements. Electrochemical measurements were conducted in a three-electrode cell using Bio-logic EC-Lab SP-300. Pt wire and Hg/HgO (1 M NaOH) were used as the counter and the reference electrodes, respectively. All electrochemical data were obtained at room temperature. To prepare the working electrode, 15 μL of the catalyst ink containing 3 μg of Pd based on inductively coupled plasma-optical emission spectrometry (ICP-OES) was dropped onto a glassy carbon electrode (GCE, diameter: 5 mm), and then dried at room temperature. The dried GCE was cleaned electrochemically by 30 potential cycles between -0.919 V and 0.281 V *vs.* Hg/HgO at a scan rate of 50 mV s^{-1} in 0.5 M KOH. The electrolyte solutions were purged with N_2 gas for 30-60 min before performing electrochemical experiments. The CVs of all catalysts were obtained between -0.919 V and 0.281 V *vs.* Hg/HgO at a scan rate of 50 mV s^{-1} in 0.5 KOH + 1 M ethanol.

III. Result and Discussion

Figure 1 displays scanning electron microscopy (SEM) and transmission electron microscopy (TEM) images of the nanostructures, indicating that a majority of produced nanostructures were ultrathin assembled nanosheets (UANs). This intrinsic morphological feature of the ultrathin assembled nanosheets (UANs) can improve the catalytic activity for various catalytic reactions. The high-resolution TEM (HRTEM) image of a ultrathin assembled nanosheet (UAN) shown in Figure 1c reveals the d-spacing of 2.24 Å between adjacent lattice fringes, which corresponds with that of the (111) planes of face centered cubic (fcc) Pd−Pt alloy. To investigate the thickness of the ultrathin assembled nanosheets, we obtained HRTEM image (figure 1d) which displays the side plane of the ultrathin assembled nanosheet (UAN). Figure 1d shows that the thickness of nanosheets in the ultrathin assembled nanosheets (UANs) was approximately 6.0 ± 0.5 nm.

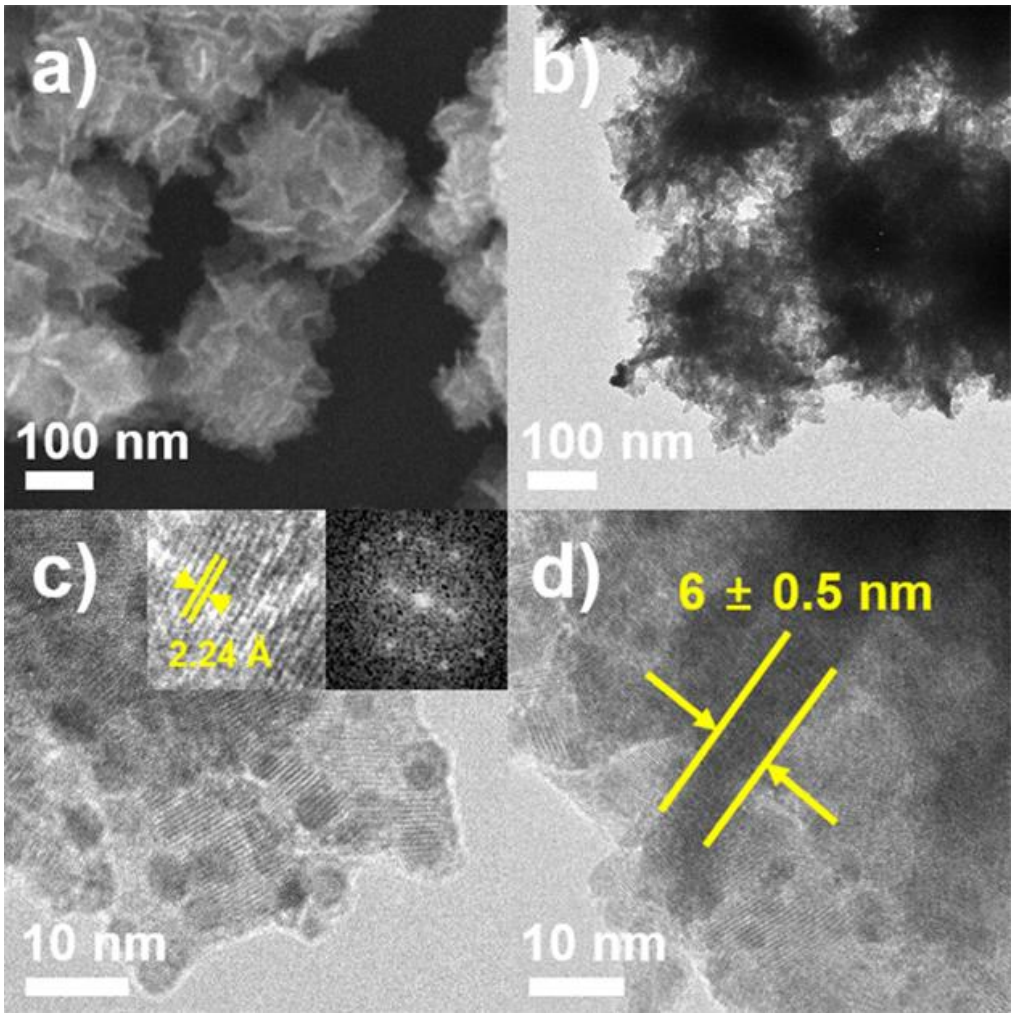

Figure 1. (a) SEM and (b) TEM, and c) HRTEM images of the Pd-Pt UANs. Insets in Figure 1c show high-magnification HRTEM image and FFT pattern obtained from a ultrathin nanosheet subunits of Pd-Pt UAN. d) HRTEM image of the side face of a ultrathin nanosheet subunit.

For an investigation of the detailed structural characteristics of the ultrathin assembled nanosheets (UANs), the high-angle annular dark field scanning TEM (HAADF−STEM) image of a ultrathin assembled nanosheet (UAN) was obtained (Figure 2). The weak contrast was observed at nanosheet parts in the ultrathin assembled nanosheet (UAN), indicating the ultrathin nanosheets of the prepared ultrathin assembled nanosheet (UAN). Overall, it shows the hierarchical shape that has particle subunit in middle side and sheet subunit around the particle. The compositional structure of the ultrathin assembled nanosheet (UAN) was measured by elemental mapping with HAADF−STEM−energy-dispersive X-ray spectroscopy (HAADF−STEM−EDS), which clearly confirmed the formation of a homogeneous Pd−Pt alloy structure. The Pd/Pt atomic ratio of the ultrathin assembled nanosheet investigated by inductive coupled plasma-optical emission spectroscopy (ICP−OES) was 91.44:8.56 (about 10:1).

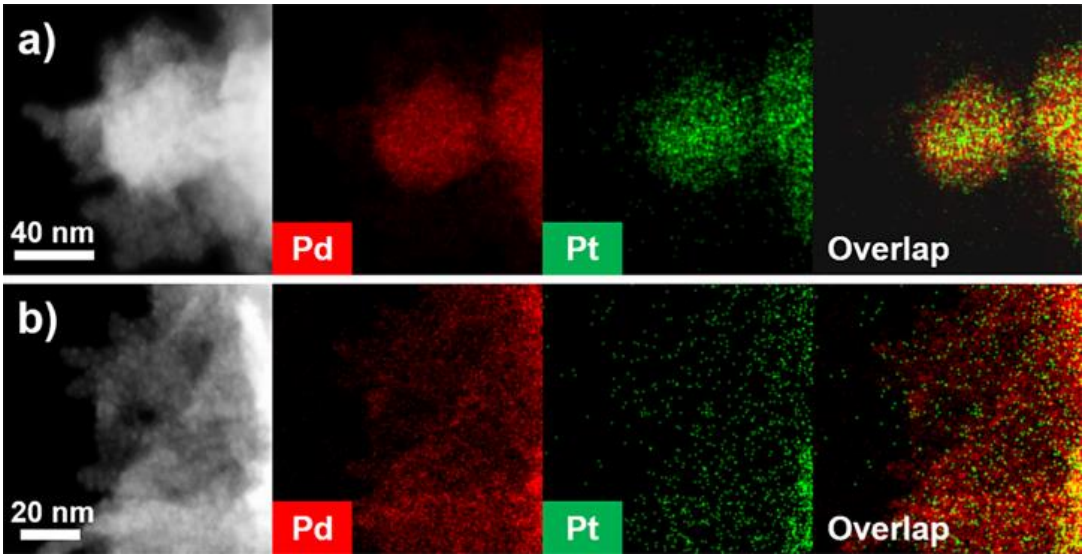

Figure 2. HAADF-STEM image and corresponding HAADF-STEM-EDS elemental mapping images of (a) Pd-Pt UANs and b) ultrathin nanosheet subunit.

The X-ray diffraction (XRD) pattern of the Pd-Pt ultrathin assembled nanosheets (**U**AN**s**) (Figure 3) exhibits the inherent peaks corresponding to cuprite structure of Pd-Pt bimetallic alloy feature. It shows noticeable five peaks at 40.0, 46.5, 68.1 and 82.1 degree (2 theta), meaning the face-centered cubic structure. Using XRD pattern, we calculate the average crystallite size of the assembled nanosheets. It obtained by the Scherrer equation (eq. 1), was 14.52 nm. It can be interpreted that single crystals of 14.52 nm form the Pd-Pt ultrathin assembled nanosheets (**U**AN**s**).

[Scherrer equation]

$$D = K \lambda / \beta (\cos \theta) \quad \text{---------- (1)}$$

D: crystallites size (nm)

K: 0.9 (Scherrer constant)

λ: 0.15406 nm (wavelength of the x-ray source)

β: FWHM (radians)

θ: peak position (radians)

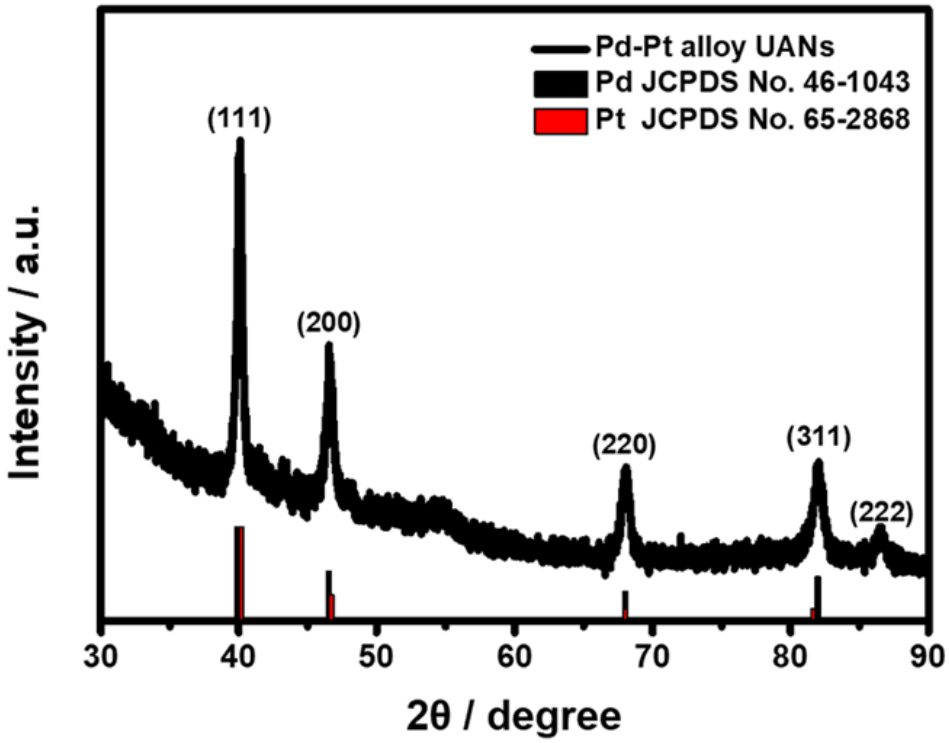

Figure 3. X-ray diffraction (XRD) pattern of the Pd-Pt UANs.

For synthesizing the Pd−Pt ultrathin assembled nanosheets (**U**AN**s**), adjusting the growth behavior of nanostructures by controlling the amount of I^- ion, AA and the concentration of CTAC are critical factor. To identify the effect of amount of I^- ion on the formation of ultrathin assembled nanosheets (**U**AN**s**), different amounts of KI (50 mM) from 0 to 4.0 mL instead of 0.8 mL used in standard synthesis for the Pd−Pd ultrathin assembled nanosheets (**U**AN**s**) were used under otherwise identical experimental conditions (Figures 4). When 0, 0.1, 0.2, and 0.4 mL of KI were employed, irregular-shaped nanostructures were obtained, while introduction of 0.8 and 1.2 mL of KI leaded the formation of ultrathin assembled nanosheets (**U**AN**s**). A further increase in the amount of KI to 1.6 and 4.0 mL induced the aggregated nanostructures. This can be elucidated to the promoted oxidative etching from halide ion/oxygen pairs due to excessive I^- ion in the reaction mixtures. These results unambiguously demonstrate that optimal amount of I^- ion can effectively promote the 2D growth of Pd and Pt by suppressing the growth of [111] orientation, which was indispensable to the formation of the Pd−Pt ultrathin assembled nanosheets (**U**AN**s**).

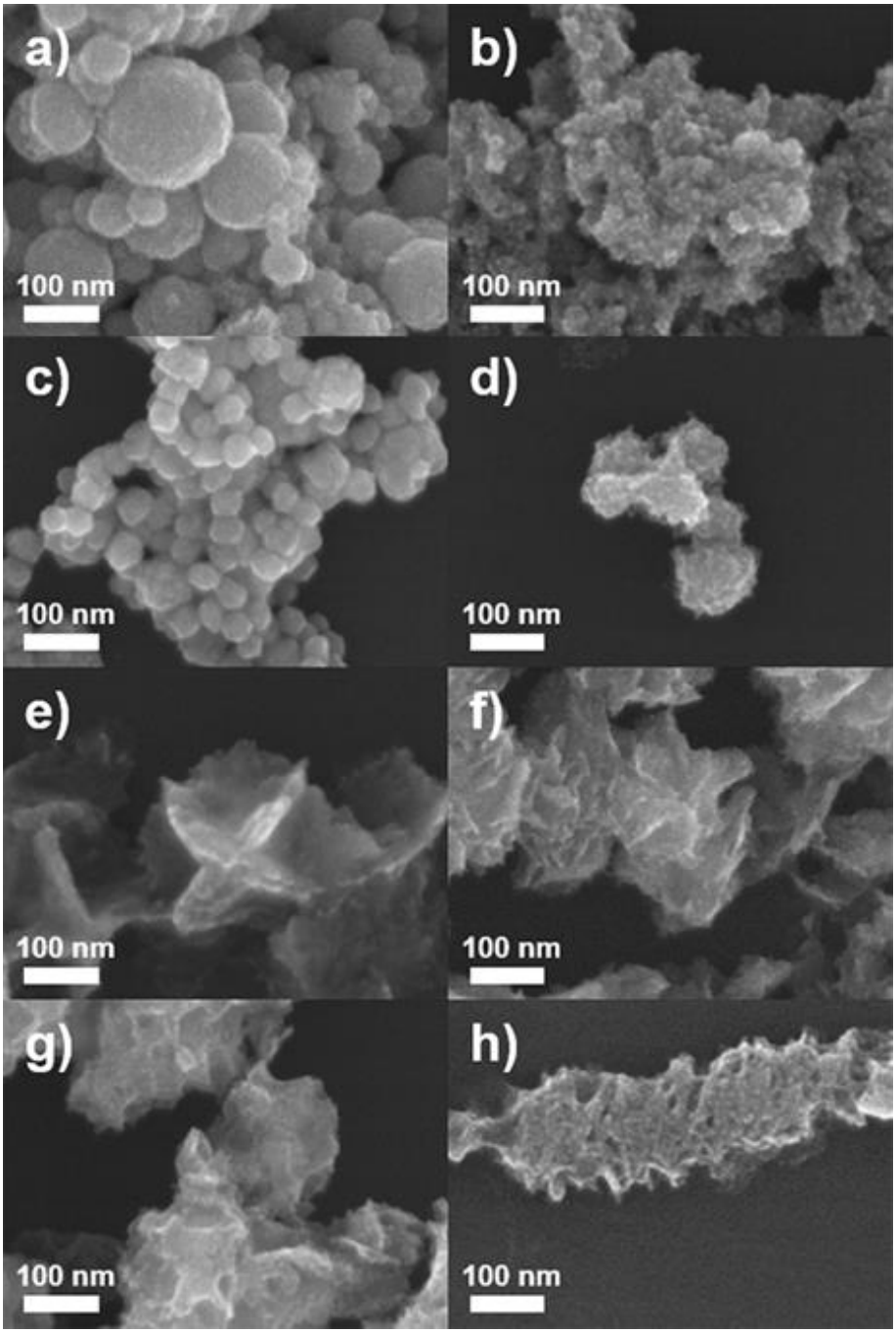

Figure 4. SEM images of NCs produced in reaction mixtures with (a-d) 0, 0.1, 0.2 and 0.4 mL, (e) 0.8 mL (standard), (f-h) 1.2, 1.6 and 4.0 mL of 50 mM KI.

Furthermore, to investigate the influence of CTAC used as surfactant for the formation of Pd−Pt ultrathin assembled nanosheets (**U**AN**s**), respectively, control experiment were performed by employing different amounts of CTAC (Figures 5). Without CTAC (1.0 mL of DIW) synthesizing, small particles were made (Figure 5a). When lower amount of CTAC (1.0 mL, 1.0 mM) than that used in the standard synthesis nanosheets, respectively, leaded the formation of Pd−Pt ultrathin assembled nanosheets (Figure 5b) with highly similar shape with standard Pd−Pt ultrathin assembled nanosheets (Figure 5c), while employing higher amount of CTAC (1.0 mL, 10, 20, 50, 100 and 200 mM) induced the 3D nanostructures with irregular shapes (Figure 5d-h).

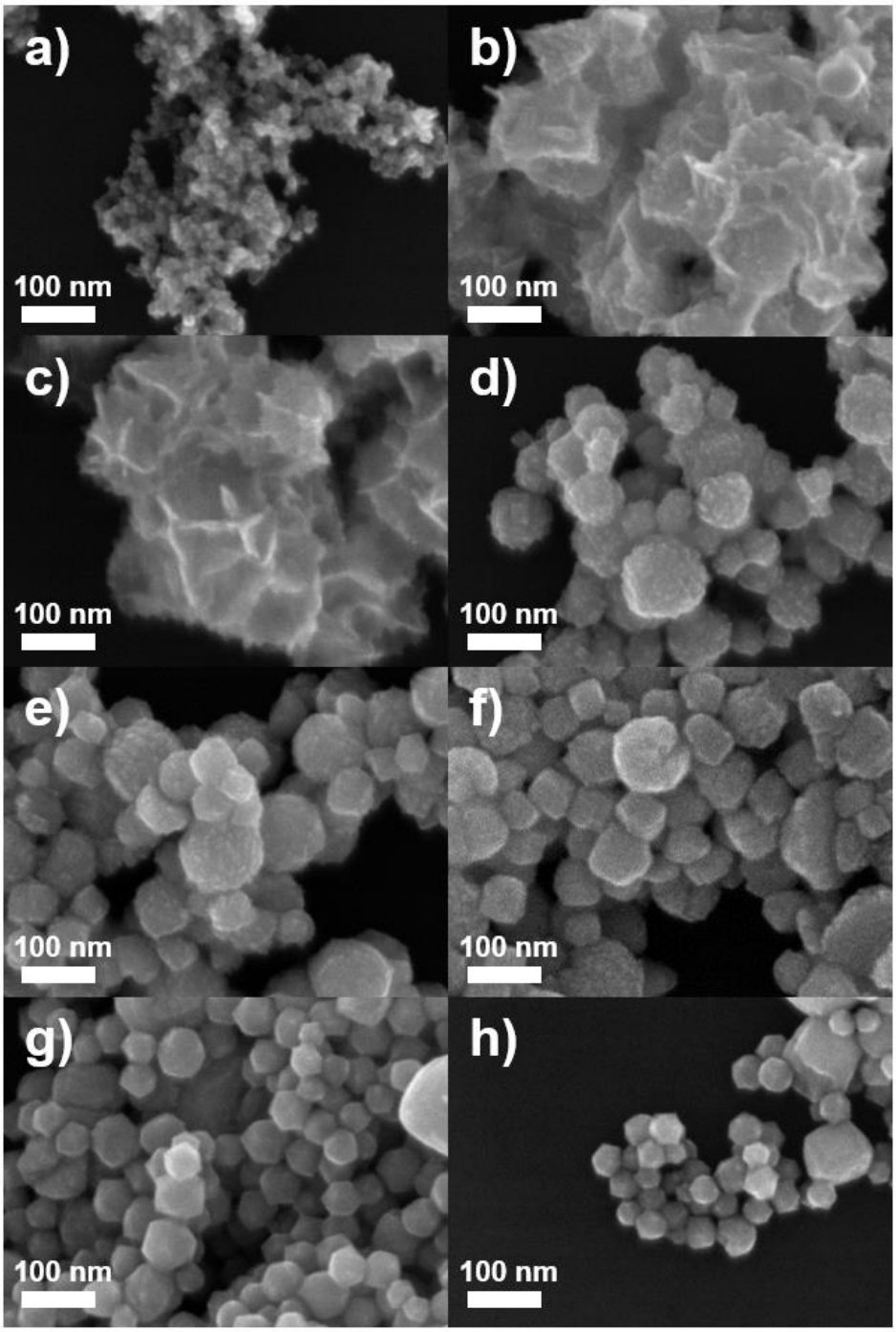

Figure 5. SEM images of NCs produced in reaction mixtures with (a-b) deionized water and 1 mM, (c) 5 mM (standard), (d-h) 10, 20, 50, 100 and 200 mM CTAC.

Similar results were observed by applying the different amount of AA in the reaction mixtures (Figure 6). The Pd−Pt ultrathin assembled nanosheets (Figure 6a-d) were obtained by using lower concentration of AA (0, 0.02, 0.05 and 0.1 mL, 50 mM) compared with that in standard condition (Figure 6e), whereas increasing the amount of AA to 1.0 and 2.0 mL produced the nanostructures with random sizes and shapes (Figure 6g-h). These results can be elucidated by attenuation of stabilizing effect of I^- ion in the high concentration of CTAC and AA. In the high concentration of CTAC, CTAC may disturb the adsorption of I^- ion on the surface of Pd-Pt nanostructures. Similarly, high concentration of AA can trigger the 3D growth of Pd-Pt, which facilitate the formation of 3D nanostructures with irregular shapes. These results of control experiments collectively validate that the synthesis of Pd−Pt assembled nanosheets with ultrathin thickness could be realized by controlling the growth behavior of Pd-Pt via modulation of the KI, CTAC, and AA concentration.

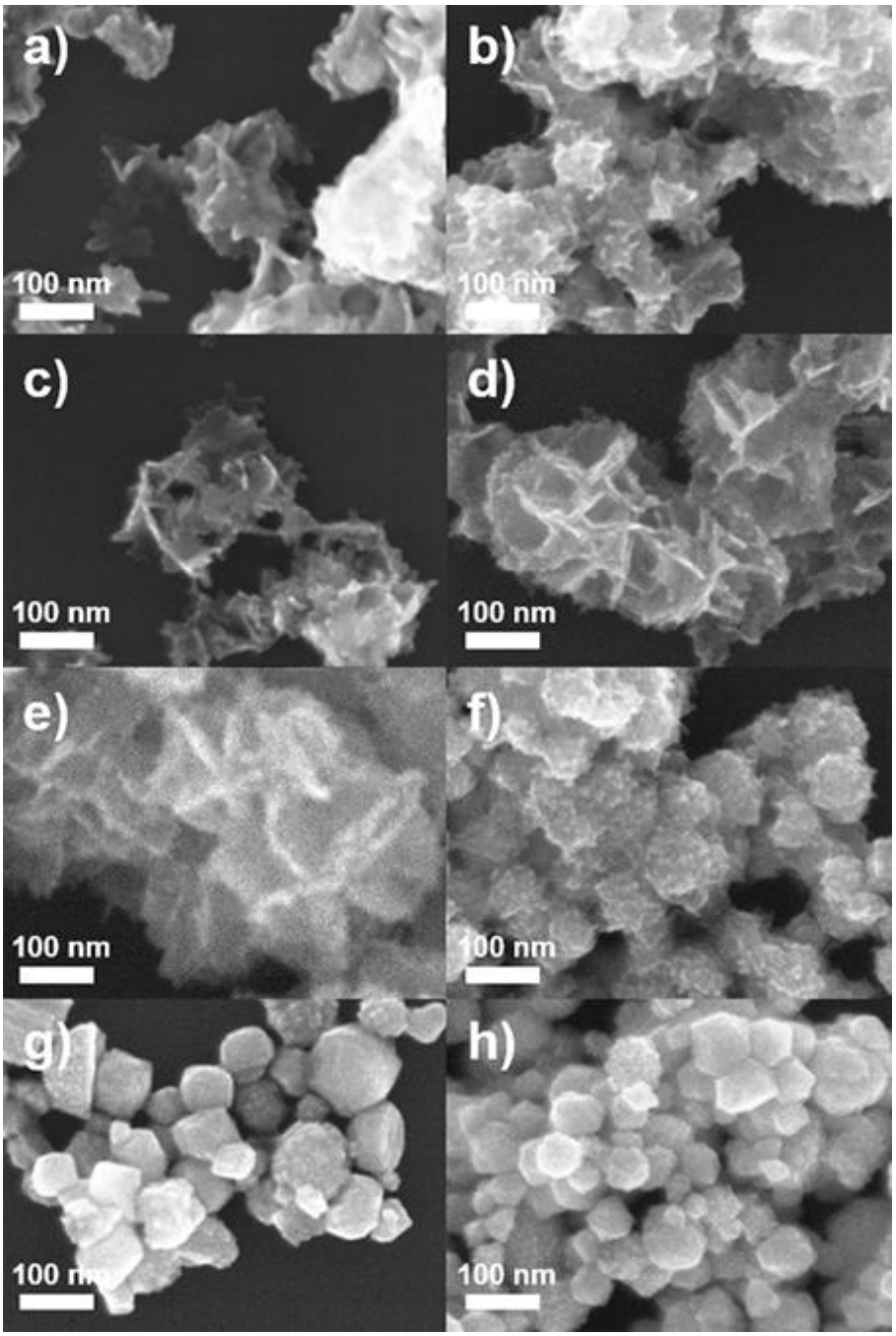

Figure 6. SEM images of NCs produced in reaction mixtures with (a-d) 0, 0.02, 0.05 and 0.1 mL (e) 0.2 mL (standard), (f-h) 0.5, 1.0, 2.0 mL of 50 mM AA.

We set standard method for synthesizing Pd-Pt ultrathin assembled nanosheets (**U**AN**s**) using 0.2 mL of 50 mM KI, 1 mL of 5 mM CTAC and 0.2 mL of 50 mM AA solution. Additionally, we synthesized Pd-Pt irregular shaped nanocrystals (IS NCs) for comparing the effect of the ultrathin nanosheet part of hierarchical shape. For preparing Pd-Pt irregular shaped nanocrystals (IS NCs), 1 mL of 10 mM CTAC solution was added into reaction mixtures instead of 1 mL of 5 mM CTAC. They have a lot of irregular and angular points. The size of Pd-Pt irregular shaped nanocrystals (IS NCs) are about 70±10 nm.

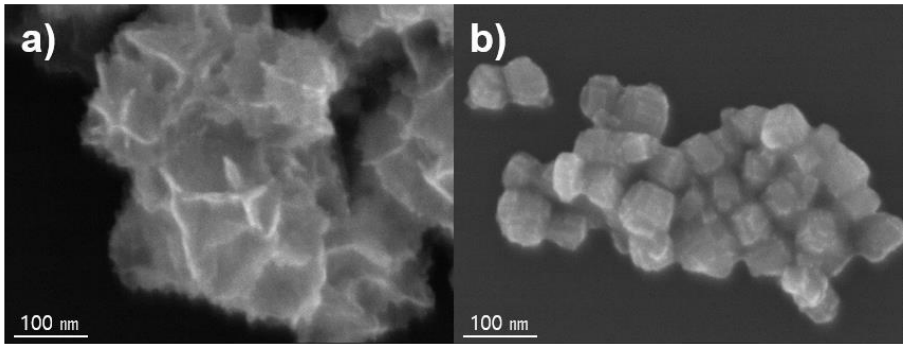

Figure 7. SEM images of (a) Pd-Pt UANs and (b) Pd-Pt IS NCs.

The Pd-Pt ultrathin assembled nanosheets (UANs) were used as electrocatalysts for ethanol oxidation reaction (EOR) to investigate their morphological benefit. The EOR activity of the Pd-Pt ultrathin assembled nanosheets (UANs) was evaluated in comparison with Pd-Pt irregular shaped nanocrystals (IS NCs), commercial Pd/C and Pt/C catalysts. The cyclic voltammograms (CVs) of different catalysts are shown in Figure 8a. Based on the integrated charge associated with cathodic peak between -0.54 and 0.10 V (vs Hg/HgO), we estimated that the electrochemically active surface areas (ECSAs) of the Pd-Pt ultrathin assembled nanosheets (UANs), Pd-Pt irregular shaped nanocrystals (IS NCs), Pt/C and Pd/C catalysts as 27.7, 14.9, 30.4 and 31.2 $m^2 g^{-1}$, respectively (normalized to the total amount of metal). Although the ECSAs value of Pd-Pt ultrathin assembled nanosheets (UANs) was less than both commercial catalysts, it was considerably larger than those of Pd-Pt irregular shaped nanocrystals (IS NCs) because of ultrathin nanosheet part. Figure 8b shows the CVs obtained for the EOR with different catalysts in 0.5 M KOH and 1.0 M ethanol. It is apparent that the Pt-Pd ultrathin assembled nanosheets (UANs) showed the highest EOR activity among the different catalysts. The mass activity of Pd-Pt ultrathin assembled nanosheets (3369 mA mg^{-1}) was 1.91, 2.36 and 2.71 times larger than those of the Pd-Pt irregular shaped nanocrystals (1767 mA mg^{-1}), Pd/C (1430 mA mg^{-1}) and Pt/C (1243 mA mg^{-1}), respectively. Moreover, the corresponding current density of the Pd-Pt ultrathin assembled nanosheets was 12.16 mA cm^{-2}, which is roughly 1.03, 2.58 and 3.05 times higher than those of the Pd-Pt irregular shaped nanocrystals (11.86 mA cm^{-2}), Pd/C (4.71 mA cm^{-2}) and Pt/C (3.99 mA cm^{-2}) catalysts, respectively (Figure 8c). By this regard, mass activities of Pd-Pt ultrathin assembled nanosheets (UANs) was higher than commercial Pd/C and Pt/C. It could indicate bimetallic catalyst makes higher activity in EOR because of compositional effect of metals. Additionally, Pd-Pt ultrathin assembled nanosheets (UANs) showed higher mass activity than Pd-Pt irregular shaped nanocrystals (IS NCs). It means that it was attributed to the large active surface areas from ultrathin nanosheet part.

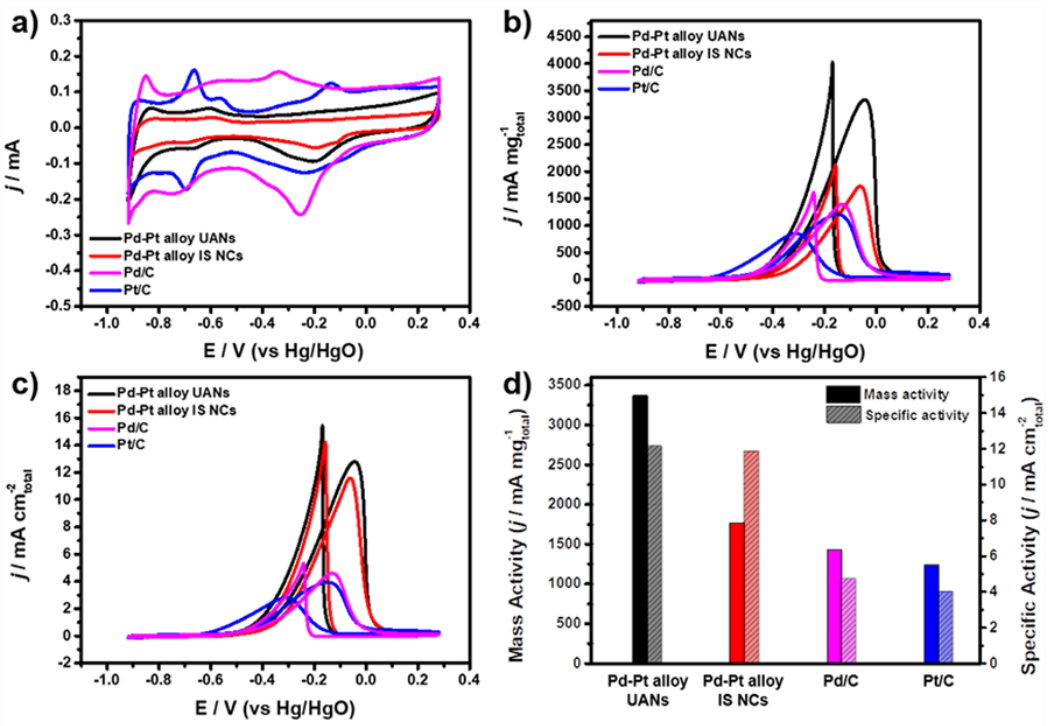

Figure 8. (a) CVs of the various catalysts on GCE in 0.5 M KOH and (b, c) in 0.5 M KOH + 1.0 M ethanol at a scan rate of 50 mV/s at room temperature. The current values were normalized with respect to the (b) total metal mass and (c) ECSA, respectively and (d) corresponding mass activities and specific activities of the various catalysts

The electrochemical stability of Pt-Pd ultrathin assembled nanosheets (UANs) was estimated by repeating CV and their properties were compared with different catalysts (Figure 9). Stability test was conducted in 0.5 M KOH + 1.0 M EtOH between -0.919 and 0.281 V (vs Hg/HgO) at a scan rate of 50 mV/s at room temperature. After 300 cycles, the mass activities of Pt-Pd ultrathin assembled nanosheets (UANs), Pd/C and Pt/C decreased from 3307 mA mg^{-1} to 2355 mA mg^{-1}, from 1375 mA mg^{-1} to 763 mA mg^{-1} and from 1315 mA mg^{-1} to 772 mA mg^{-1}, which signifies losses of 28.8, 44.5 and 41.3% in mass activity, respectively. The Pd-Pt ultrathin assembled nanosheets (UANs) shows the best stability among the different catalysts of EOR activity. It contains the activity over 70 % after 300 cycles, which takes 4 h.

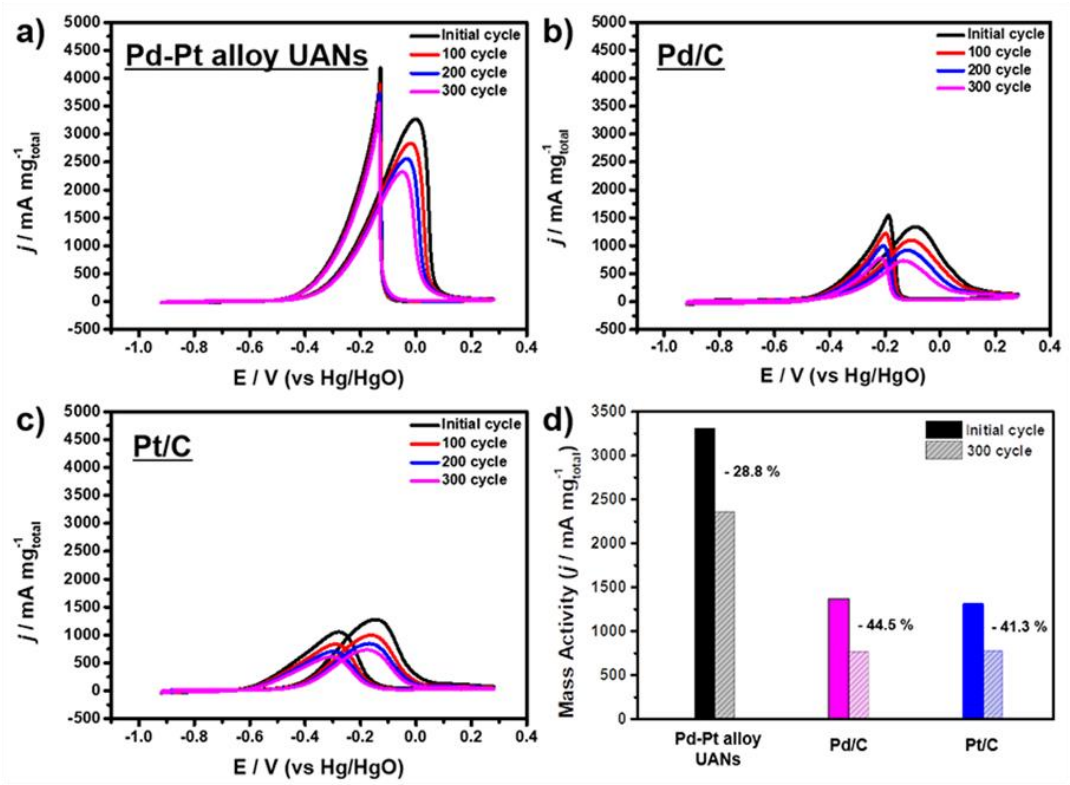

Figure 9. CVs obtained before and after stability test for a) Pd-Pt UANs, b) Pd/C, and c) Pt/C catalysts in 0.5 M KOH + 1.0 M ethanol at a scan rate of 50 mV/s. d) mass activities of various catalysts before and after stability test.

IV. Conclusion

In summary, Pt-Pd ultrathin assembled nanosheets (UANs) have been prepared through a facile wet-chemical synthesis. The modulated growth behavior of Pt-Pd nanostructures by introduction of optimal concentration of KI, CTAC, and AA is a critical point for successful production of Pt-Pd ultrathin assembled nanosheets (UANs) because 3D growth of Pt-Pd could be effectively suppressed in the optimal condition. Of various catalysts including Pt-Pd ultrathin assembled nanosheets (UANs), Pd-Pt irregular shaped nanocrystals (IS NCs), Pd/C and Pt/C catalysts, the Pt-Pd ultrathin assembled nanosheets (UANs) exhibited remarkable catalytic activity and stability for the EOR compared to the other different catalysts by both low-coordinated and Pt-Pd alloy surfaces. This shows the significance of morphology and composition engineering of nanostructures with potential applications for various electrocatalysis.

V. References

1. Shafiee, Shahriar, and Erkan Topal. "When will fossil fuel reserves be diminished?." Energy policy 37, no. 1 (2009): 181-189.
2. Cerritos, Raúl Carrera, Minerva Guerra-Balcázar, Rosalba Fuentes Ramírez, Janet Ledesma-García, and Luis Gerardo Arriaga. "Morphological effect of Pd catalyst on ethanol electro-oxidation reaction." Materials 5, no. 9 (2012): 1686-1697.
3. Demirbas, M. Fatih, Mustafa Balat, and Havva Balat. "Biowastes-to-biofuels." Energy Conversion and Management 52, no. 4 (2011): 1815-1828.
4. L. J. M. J. Blomen and M. N. Mugerwa, "Fuel Cell Systems", Plenum Press, New York, 1993.
5. K. Kordesch and G. Simader, "Fuel Cells and Their Applications", VCH, Weinheim, Germany, 1996.
6. Shibata, Masami, and Satoshi Motoo. "Electrocatalysis by ad-atoms: part XXI. Catalytic effects on the elementary steps in methanol oxidation by non-oxygen-adsorbing ad-atoms." Journal of electroanalytical chemistry and interfacial electrochemistry 229, no. 1-2 (1987): 385-394.
7. Kang, Shin Wook, Young Wook Lee, Minjung Kim, Jong Wook Hong, and Sang Woo Han. "One-Pot Synthesis of Carbon-Supported Dendritic Pd-Au Nanoalloys for Electrocatalytic Ethanol Oxidation." Chemistry–An Asian Journal 6, no. 3 (2011): 909-913.
8. Mazumder, Vismadeb, Youngmin Lee, and Shouheng Sun. "Recent development of active nanoparticle catalysts for fuel cell reactions." Advanced Functional Materials 20, no. 8 (2010): 1224-1231.
9. Zhang, Zhiyong, Le Xin, Kai Sun, and Wenzhen Li. "Pd–Ni electrocatalysts for efficient ethanol oxidation reaction in alkaline electrolyte." International Journal of Hydrogen Energy 36, no. 20 (2011): 12686-12697.
10. Zhao, T. S., Y. S. Li, and S. Y. Shen. "Anion-exchange membrane direct ethanol fuel cells: Status and perspective." Frontiers of Energy and Power Engineering in China 4, no. 4 (2010): 443-458.
11. Ge, Junjie, Wei Xing, Xinzhong Xue, Changpeng Liu, Tianhong Lu, and Jianhui Liao. "Controllable synthesis of Pd nanocatalysts for direct formic acid fuel cell (DFAFC)

application: from Pd hollow nanospheres to Pd nanoparticles." The Journal of Physical Chemistry C 111, no. 46 (2007): 17305-17310.

12. Mazumder, Vismadeb, and Shouheng Sun. "Oleylamine-mediated synthesis of Pd nanoparticles for catalytic formic acid oxidation." Journal of the American Chemical Society 131, no. 13 (2009): 4588-4589.
13. Huang, Xiaoqing, Shaoheng Tang, Huihui Zhang, Zhiyou Zhou, and Nanfeng Zheng. "Controlled formation of concave tetrahedral/trigonal bipyramidal palladium nanocrystals." Journal of the American Chemical Society 131, no. 39 (2009): 13916-13917.
14. Ksar, Faycal, Geetarani Surendran, Laurence Ramos, Bineta Keita, Louis Nadjo, Eric Prouzet, Patricia Beaunier, Agnes Hagege, Fabrice Audonnet, and Hynd Remita. "Palladium nanowires synthesized in hexagonal mesophases: application in ethanol electrooxidation." Chemistry of Materials 21, no. 8 (2009): 1612-1617. C. Xu, H. Wang, P. K. Shen, S. P. Jiang, Adv. Mater. 2007, 19, 4256.
15. N. Tian, Z.-Y. Zhou, S.-G. Sun, Chem. Commun. 2009, 1502.
16. Cui, Guofeng, Shuqin Song, Pei Kang Shen, Andrzej Kowal, and Claudio Bianchini. "First-principles considerations on catalytic activity of Pd toward ethanol oxidation." The Journal of Physical Chemistry C 113, no. 35 (2009): 15639-15642.
17. Kim, Heon Chul, Yena Kim, Yoshio Bando, Yusuke Yamauchi, and Jong Wook Hong. "Shape-controlled Pd nanocrystal–polyaniline heteronanostructures with modulated polyaniline thickness for efficient electrochemical ethanol oxidation." Journal of Materials Chemistry A 7, no. 38 (2019): 22029-22035.
18. Hong, Jong Wook, Yena Kim, Dae Han Wi, Seunghoon Lee, Su-Un Lee, Young Wook Lee, Sang-Il Choi, and Sang Woo Han. "Ultrathin free-standing ternary-alloy nanosheets." Angewandte Chemie International Edition 55, no. 8 (2016): 2753-2758.
19. Zhu, Enbo, Xucheng Yan, Shiyi Wang, Mingjie Xu, Chen Wang, Haotian Liu, Jin Huang et al. "Peptide-Assisted 2-D Assembly toward Free-Floating Ultrathin Platinum Nanoplates as Effective Electrocatalysts." Nano letters 19, no. 6 (2019): 3730-3736.
20. Ye, Wei, Shuangming Chen, Mengshan Ye, Chenhao Ren, Jun Ma, Ran Long, Chengming Wang, Jian Yang, Li Song, and Yujie Xiong. "Pt4PdCu0. 4 alloy nanoframes as highly efficient and robust bifunctional electrocatalysts for oxygen reduction reaction and formic acid oxidation." Nano Energy 39 (2017): 532-538.

21. Bu, Lingzheng, Nan Zhang, Shaojun Guo, Xu Zhang, Jing Li, Jianlin Yao, Tao Wu et al. "Biaxially strained PtPb/Pt core/shell nanoplate boosts oxygen reduction catalysis." Science 354, no. 6318 (2016): 1410-1414.
22. Hong, Jong Wook, Shin Wook Kang, Bu-Seo Choi, Dongheun Kim, Sang Bok Lee, and Sang Woo Han. "Controlled synthesis of Pd–Pt alloy hollow nanostructures with enhanced catalytic activities for oxygen reduction." ACS nano 6, no. 3 (2012): 2410-2419.
23. Jo, Yu-Geun, Sung-Min Kim, Jung-Wan Kim, and Sang-Yul Lee. "Composition-tuned porous Pd-Ag bimetallic dendrites for the enhancement of ethanol oxidation reactions." Journal of Alloys and Compounds 688 (2016): 447-453.
24. Zheng, Yuanyuan, Junhua Qiao, Junhua Yuan, Jianfeng Shen, Ai-jun Wang, and Shengtang Huang. "Controllable synthesis of PtPd nanocubes on graphene as advanced catalysts for ethanol oxidation." International Journal of Hydrogen Energy 43, no. 10 (2018): 4902-4911.